Electronic Supplementary Material (ESI) for Sustainable Energy & Fuels.

In situ fabrication of self-assembly $BiOBr_xI_{1-x}$ coated on carbon nanofiber for efficient solar light-driven photocatalytic nitrogen fixation

Chenghe Hua, Xiaoli Dong*, Nan Zheng, Xinxin Zhang and Mang Xue

School of Light Industry and Chemical Engineering, Dalian Polytechnic University, #1 Qinggongyuan, Dalian 116034, P R China

*Corresponding author：dongxiaoli65@163.com

Experimental

Electrochemical test

Photoelectrochemical (PEC) measurements were carried out on a CHI660E electrochemical workstation (Shanghai Chenhua, P. R. China) operated with a three-electrode configuration. An aqueous solution of 0.5 M Na_2SO_4 was used as electrolyte. For preparing working electrode, 5 mg sample was suspended in the mixture of 10 μL Nafion solution (D520, DuPont), 1.5 mL ethanol and 0.5 mL ultrapure water to become slurry, which was then dip-coated onto a glass carbon electrode and dried in the shade. The light source is a 300 W Xe lamp (PLS-SXE 300, Beijing Perfect Light Co., Ltd.). The photocurrent response was obtained by potentiostatic (current vs. time, *I-t*) measurements under intermittent illumination (30 s) in the condition of no bias potential. Electrochemical impedance spectroscopy (EIS) was conducted with an alternating current signal (10 mV) in the frequency range of 0.1-10^5 Hz at open circuit potential (OCP). Mott-Schottky plots were measured at a frequency of 1000 Hz in the dark. The polarization curves were tested via linear sweep voltammetry (LSV) at a scan rate of 100 mV• s^{-1}.

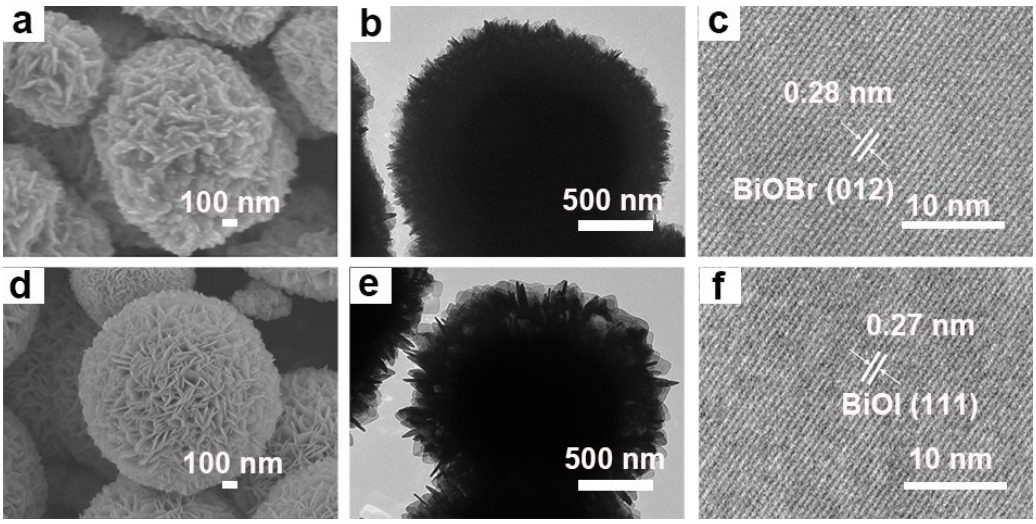

Fig. S1 (a-c) SEM and TEM images of BiOBr, (d-f) SEM and TEM images of BiOI

Fig. S1c shows the HRTEM of the BiOBr, and the lattice figures are presented with the lattice spaces of 0.28 nm, which could be indexed to (012) lattice plane of BiOBr. Meanwhile, HRTEM images (Fig. S1f) shows the lattice fringes with the d-spaces of 0.27 nm, in accordance of the (111) lattice plane of BiOI.

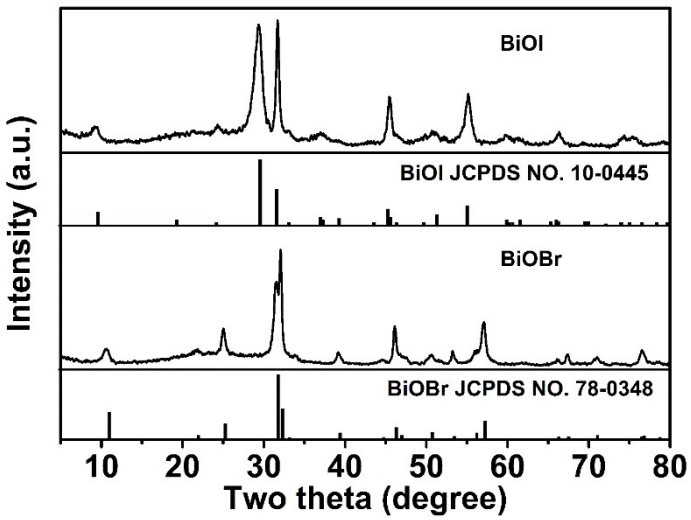

Fig. S2 XRD patterns of BiOBr and BiOI

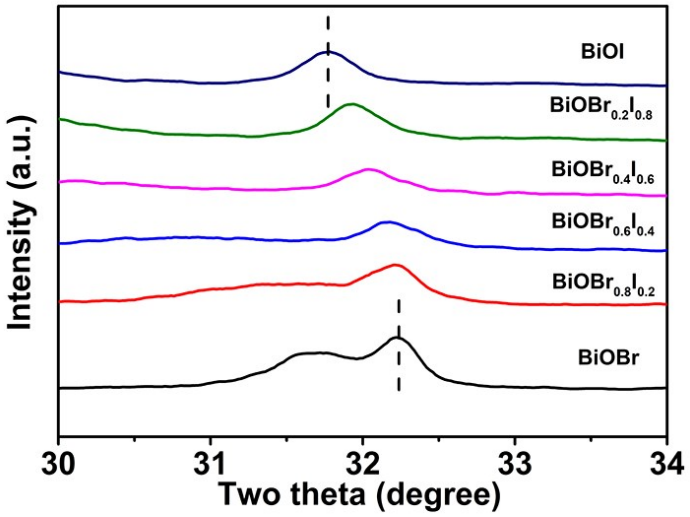

Fig. S3 The amplified XRD patterns of $BiOBr_xI_{1-x}$

The amplified XRD patterns (Fig. S3) in the range of 2θ from 30° to 34°, the diffraction peak at 2θ=32.3° corresponding to (110) crystal planes of BiOBr in $BiOBr_xI_{1-x}$ is slightly shift to lower angles compared to BiOBr with the increase of I content. The slightly shift to lower angles of the (110) peak may be caused by the introduction of I, because the ionic radius of I (2.20 Å) is larger than that of Br (1.95 Å).

Table S1 The ratio of Br and I determined by EDS

samples	Concentration (Br Wt%)	Concentration (I Wt%)	Molar ratio (Br:I)
$BiOBr_{0.8}I_{0.2}$	17.62	6.643	4.21
$BiOBr_{0.6}I_{0.4}$	10.78	11.36	1.51
$BiOBr_{0.4}I_{0.6}$	8.18	18.961	0.68
$BiOBr_{0.2}I_{0.8}$	3.733	23.624	0.25

Table S2 The absorption edges and the Eg values of different samples

samples	absorption edges (nm)	Eg values (V)	samples	absorption edges (nm)	Eg values (V)
BiOBr	428	3.01	BiOBr/CNF	453	2.93
$BiOBr_{0.8}I_{0.2}$	514	2.64	$BiOBr_{0.8}I_{0.2}$/CNF	522	2.59
$BiOBr_{0.6}I_{0.4}$	564	2.38	$BiOBr_{0.6}I_{0.4}$/CNF	626	2.28
$BiOBr_{0.4}I_{0.6}$	588	2.24	$BiOBr_{0.4}I_{0.6}$/CNF	634	2.18
$BiOBr_{0.2}I_{0.8}$	618	2.12	$BiOBr_{0.2}I_{0.8}$/CNF	671	2.15
BiOI	653	2.00	BiOI/CNF	709	1.96

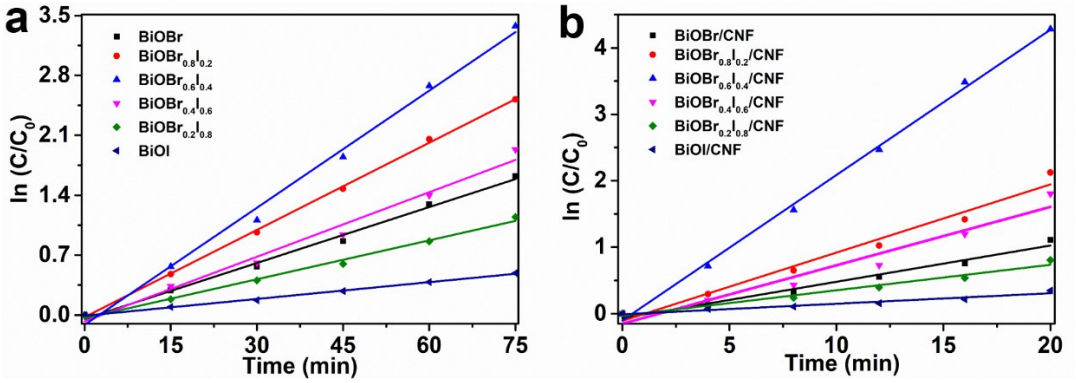

Fig. S4 the kinetic fit for degradation of RhB over the as-obtained samples

Table S3 The kinetic constants of different samples

samples	kinetic constants/min^{-1} (for RhB degradation)	samples	kinetic constants/min^{-1} (for RhB degradation)
BiOBr	0.02178	BiOBr/CNF	0.05463
$BiOBr_{0.8}I_{0.2}$	0.03397	$BiOBr_{0.8}I_{0.2}$/CNF	0.10268
$BiOBr_{0.6}I_{0.4}$	0.04561	$BiOBr_{0.6}I_{0.4}$/CNF	0.2188
$BiOBr_{0.4}I_{0.6}$	0.02514	$BiOBr_{0.4}I_{0.6}$/CNF	0.0879
$BiOBr_{0.2}I_{0.8}$	0.01515	$BiOBr_{0.2}I_{0.8}$/CNF	0.03845
BiOI	0.00654	BiOI/CNF	0.01588

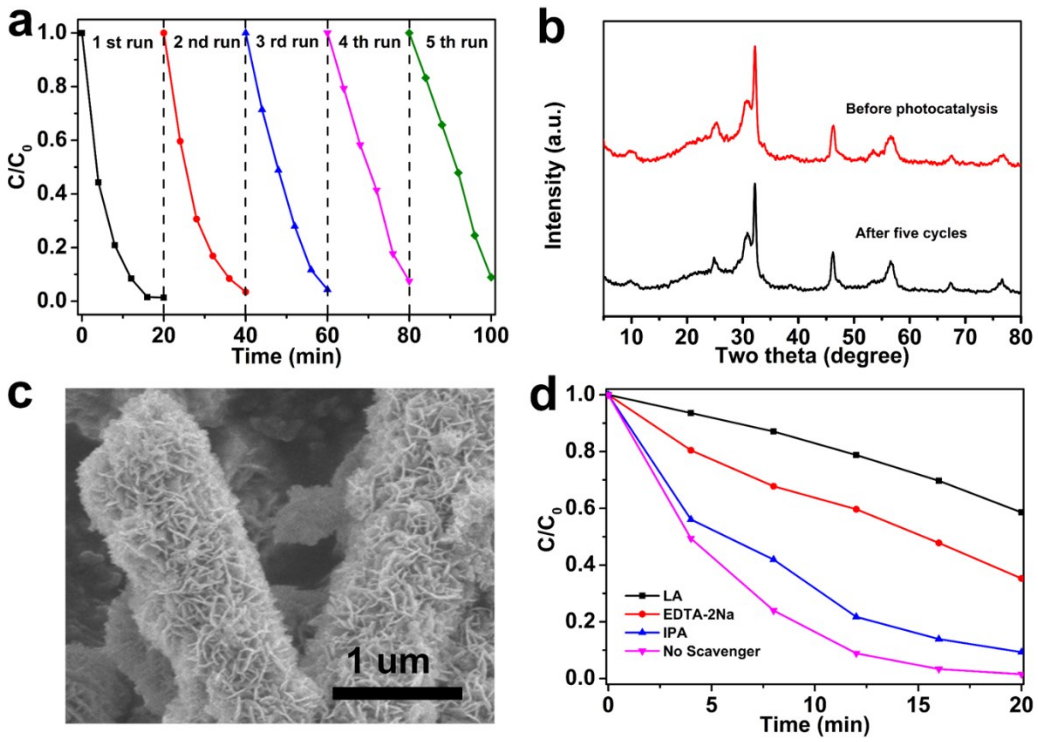

Fig. S5 (a) cycling runs of $BiOBr_{0.6}I_{0.4}$/CNF for RhB degradation under visible light, (b) XRD patterns of $BiOBr_{0.6}I_{0.4}$/CNF before and after photocatalytic experiments, (c) The SEM image of $BiOBr_{0.6}I_{0.4}$/CNF sample after photocatalytic experiments, (d) Photocatalytic performances of $BiOBr_{0.6}I_{0.4}$/CNF with different scavengers

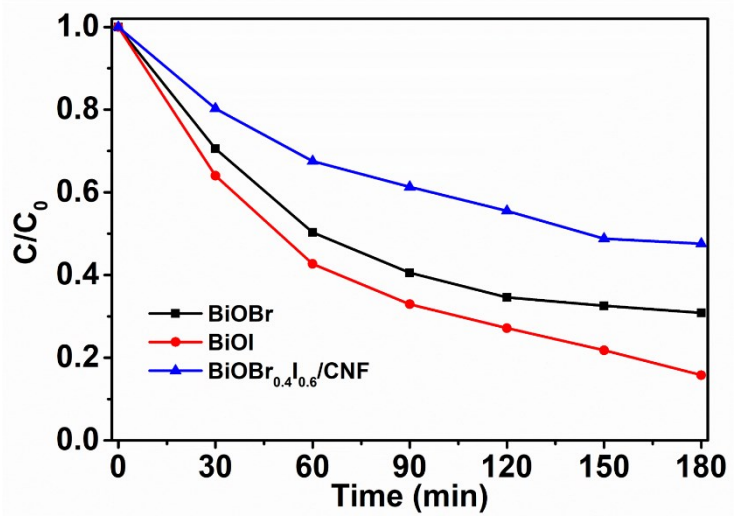

Fig. S6 Concentration changes of tetracycline over different photocatalysts

Table S4 The photocatalytic N_2 fixation rate of different samples

samples	photocatalytic N_2 fixation rate /μmol $NH_3 \bullet g^{-1} \bullet h^{-1}$	samples	photocatalytic N_2 fixation rate /μmol $NH_3 \bullet g^{-1} \bullet h^{-1}$
BiOBr	81.7	BiOBr/CNF	122.4
$BiOBr_{0.8}I_{0.2}$	135.3	$BiOBr_{0.8}I_{0.2}$/CNF	186.4
$BiOBr_{0.6}I_{0.4}$	187.5	$BiOBr_{0.6}I_{0.4}$/CNF	281.2
$BiOBr_{0.4}I_{0.6}$	109.4	$BiOBr_{0.4}I_{0.6}$/CNF	144.3
$BiOBr_{0.2}I_{0.8}$	67.7	$BiOBr_{0.2}I_{0.8}$/CNF	104.2
BiOI	51.5	BiOI/CNF	78.1

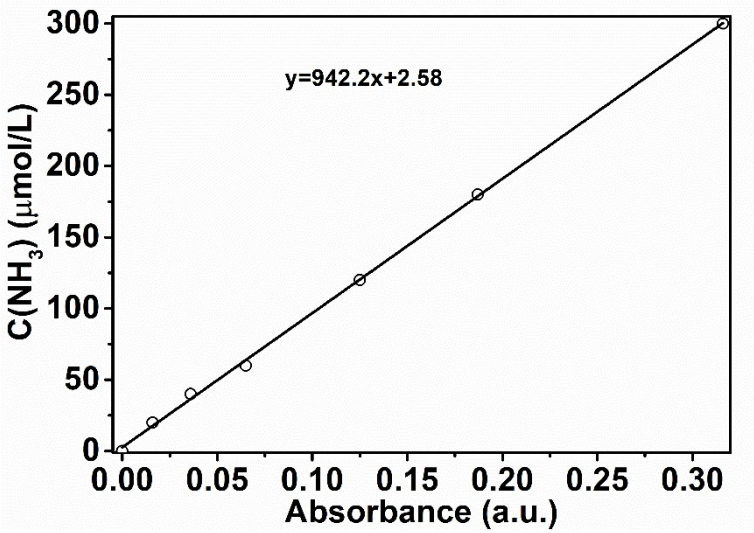

Fig. S7 Standard curve of NH_3 with Nessler's regent.

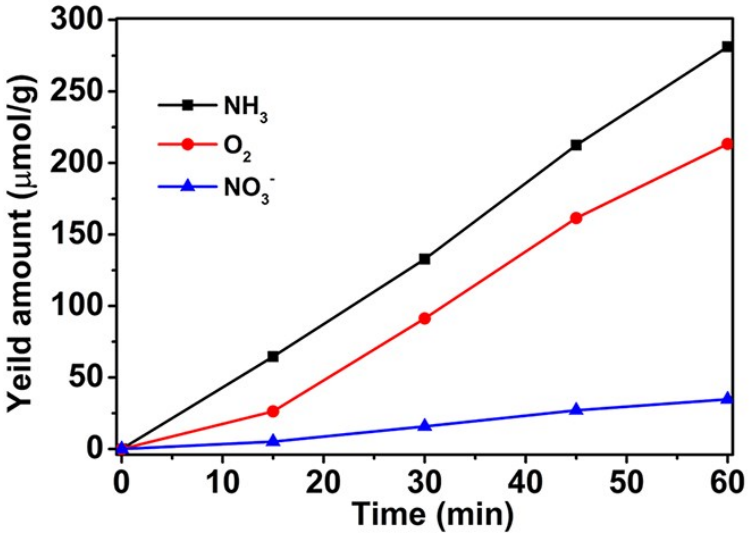

Fig. S8 Photocatalytic N_2 fixation along with the O_2 evolution and NO_3^- generation.

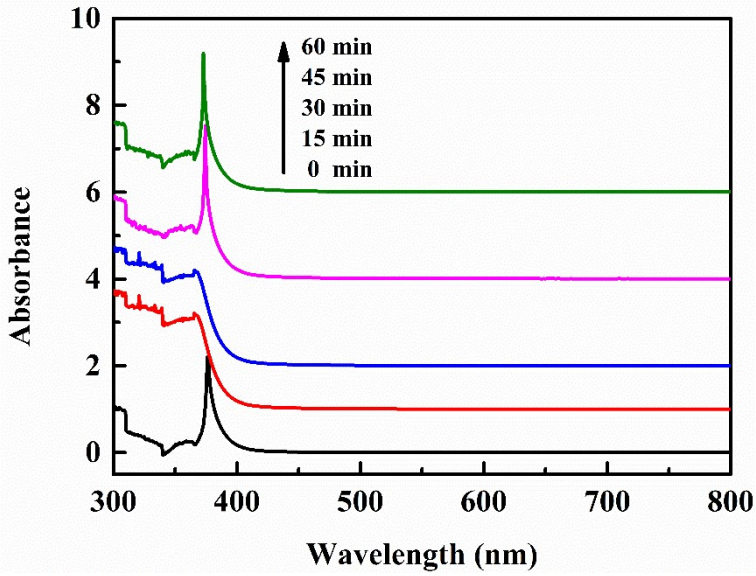

Fig. S9. The visible absorption spectra of the ammonia generation.